Transition probability from matter-wave soliton to chaos

Qianquan Zhu, Wenhua Hai,* and Shiguang Rong
Department of Physics and Key Laboratory of Low-Dimensional Quantum Structures and Quantum Control of Ministry of Education, Hunan Normal University, Changsha 410081, China

(Received 14 June 2008; revised manuscript received 8 May 2009; published 7 July 2009)

For a Bose-Einstein condensate loaded into a weak traveling optical superlattice, it is demonstrated that under a stochastic initial set and in a given parameter region, the solitonic chaos appears with a certain probability. Effects of the lattice depths and wave vectors on the chaos probability are investigated analytically and numerically and different chaotic regions associated with different chaos probabilities are found. The results suggest a method for weakening or strengthening chaos by modulating the moving superlattice.

DOI: 10.1103/PhysRevE.80.016203 PACS number(s): 05.45.Mt, 05.45.Ac, 05.45.Gg, 03.75.Kk

I. INTRODUCTION

Many phenomena observed in Bose-Einstein condensates (BECs) are well modeled by the Gross-Pitaevskii equation (GPE) [e.g., the nonlinear Schrödinger equation (NLSE)], which include chaos [1–3], soliton [4–7], and other nonlinear phenomena. As one of the most attractive topics, chaotic soliton behavior was studied previously in a NLSE with a periodic perturbation [8–10]. Lately, chaotic dynamics of soliton in BEC systems has been under intense investigation. Some of the highlights contain the chaos and energy exchange [11], the discrete soliton and chaotic dynamics in an array of BECs [12], and the bright matter-wave soliton collision [13]. Recently, the investigation is extended to BECs held in the periodic [14,15] and quasiperiodic [16–18] optical superlattices, which are in close analogies with the supercrystals and quasicrystals [19], respectively. On the other hand, a BEC interacting with a traveling lattice has also been treated experimentally [20,21] and theoretically [22–24] that shows many interesting results such as the lensing effect [21], gap soliton generation [22], and the spatiotemporal chaos [23,24]. Thus we get a physical motivation, namely, using a moving optical superlattice to study the transitions from soliton to chaos in BEC matter.

It is well known that for the fixed system parameters and the stochastic initial and boundary conditions, chaos does not always appear in a chaotic system [23], but emerges with certain probability. The chaos probability may play a significant role for the applications of chaos. Many works have focused on suppressing chaos which results in zero chaos probability. Whereas, in some realistic applications such as secure communication based on chaos [25], higher chaoticity is desired [26], which calls for higher chaos probability. In this paper, we define the chaos probability and show that in a BEC system perturbed by a moving optical superlattice consists of two lattices with different depths and wave vectors; the superlattice can separate the chaotic region into several parts with different chaos probabilities. Furthermore, for a fixed first lattice, the adjustment to the secondary lattice could turn the chaos probability to zero or higher one. The results suggest a method for weakening or strengthening chaos. Such a method can be applied to investigate the spatial chaos with zero traveling velocity and the temporal chaos in other systems.

We consider the superlattice in the form [27]

$$V_{op}(\zeta) = V_1 \cos^2(k\zeta) + V_2 \cos^2(\gamma k\zeta + \phi), \tag{1}$$

where $V_1 \cos^2(k\zeta)$ is the primary lattice with V_1 and k corresponding to its depth and wave vector and $V_2 \cos^2(\gamma k\zeta+\phi)$ is the secondary one with V_2 being its depth, γ the ratio of the two laser wave vectors, and ϕ the phase difference. The spatiotemporal variable $\zeta=x+v_L t$ contains the velocity of the traveling lattice $v_L=\delta/(2k)$ with δ being the frequency difference between the two counterpropagating laser beams producing the first lattice. The laser frequencies and amplitudes can be controlled independently by using the acousto-optic modulators [20].

II. CHAOTIC SOLITONS

For the quasi-one-dimensional (1D) BEC held in superlattice potential $V_{op}(\zeta)$, the transverse wave function is approximately in ground state of a harmonic oscillator of frequency ω_r and the governing time-dependent GPE reads

$$i\hbar \frac{\partial \Psi}{\partial t} = -\frac{\hbar^2}{2m}\frac{\partial^2 \Psi}{\partial x^2} + g_{1d}|\Psi|^2\Psi + V_{op}(\zeta)\Psi. \tag{2}$$

Here Ψ is the order parameter or is called the macroscopic quantum wave function, m is the atomic mass, and $g_{1d}=2\hbar\omega_r a_s$ characterizes the 1D interatomic interaction strength [28] with a_s being the s-wave scattering length. Mathematically, it is well known that any partial differential equation, e.g., Eq. (2), has three kinds of solutions, namely, the general solutions, complete solutions, and special solutions. Any general solution contains some arbitrary functions and any complete solution contains some arbitrary integration constants. According to the uniqueness theorem, both the general and complete solutions can be determined to the same special solution uniquely by the suitable definite conditions (e.g., enough initial and boundary conditions). It is difficult to derive the general solutions from Eq. (2). Therefore we have to seek the complete solutions. A useful method for finding the complete solutions is the separation of variables, which has been applied to solve many problems [29].

*Corresponding author; whhai2005@yahoo.com.cn

After the variable separation, a partial differential equation could be reduced to several ordinary differential equations whose solutions contain the arbitrary integration constants. Particularly, analytical investigation of chaos is very hard for a nonlinear partial differential equation due to the complete lack of analytical criterion for chaos. The unique criterion for the onset of chaos is the Melnikov criterion based on the ordinary differential equations [1,30,31]. Therefore, in order to demonstrate the soliton-chaos behaviors of Eq. (2) analytically, we have to consider the complete solutions governed by the reduced ordinary differential equations as follows.

We select the traveling-wave solution in the form of variable separation [23]

$$\Psi(x,t) = \tilde{R}[\zeta(x,t)]e^{i\{\theta[\zeta(x,t)]+\alpha x+\beta t\}}, \tag{3}$$

where $\tilde{R}(\zeta)$ and $\theta(\zeta)$ are real functions of variable ζ, another independent variable is $\alpha x+\beta t$ with two undetermined real constants α and β. Inserting Eq. (3) into Eq. (2), we easily obtain two coupled ordinary differential equations

$$\frac{d^2R}{d\xi^2} - R\left(\frac{d\theta}{d\xi}\right)^2 - (v+2\tilde{\alpha})R\frac{d\theta}{d\xi} - (\tilde{\beta}+\tilde{\alpha}^2)R - g_1R^3 = [\tilde{V}_1\cos^2(k\xi) + \tilde{V}_2\cos^2(\gamma k\xi+\phi)]R, \tag{4}$$

$$R\frac{d^2\theta}{d\xi^2} + 2\frac{dR}{d\xi}\frac{d\theta}{d\xi} + (v+2\tilde{\alpha})\frac{dR}{d\xi} = 0. \tag{5}$$

In the formulas, we have used the dimensionless variables and parameters $\xi=k_0\zeta$, $R=\tilde{R}/(10\sqrt{k_0})$, $v=2mv_L/(\hbar k_0)$, $\tilde{\alpha}=\alpha/k_0$, $\tilde{\beta}=\hbar\beta/E_{r0}$, $\tilde{V}_1=V_1/E_{r0}$, $\tilde{V}_2=V_2/E_{r0}$, $E_{r0}=\hbar^2k_0^2/(2m)$, and $g_1=400a_s/(k_0l_r^2)$, with k_0 being the unit of wave vector k and $l_r=\sqrt{\hbar/(m\omega_r)}$ the radial length of harmonic oscillator. The physical parameters have a wide range of values in experiment. We will select the suitable values as $k_0=2\pi/1047$ $(\mathrm{nm})^{-1}=6\times10^6$ m^{-1}, $v_L=3$ cm/s, $a_s=-7.5$ nm, $\omega_r=2.74$ kHz, $\alpha=6\times10^5$ m^{-1}, $\beta=2.76\times10^5$ Hz, and $m=23m_p$, with m_p the proton mass that leads to the parameters $l_r=1$ μm, $E_{r0}=5.2\times10^{-30}$ J, $v=3.6$, $\tilde{\alpha}=0.1$, $\tilde{\beta}=5.6$, and $g_1=-0.5$. For the purpose of adjustment, we let the dimensionless laser parameters k and $\tilde{V}_i$ vary their values in the given units k_0 and E_{r0}, respectively.

Integrating Eq. (5) yields $d\theta/d\xi=C/R^2-(v/2+\tilde{\alpha})$, where C is the integration constant. Applying this to Eq. (4), we arrive at the decoupled equation

$$\frac{d^2R}{d\xi^2} - \frac{C^2}{R^3} + DR - g_1R^3 = [\tilde{V}_1\cos^2(k\xi) + \tilde{V}_2\cos^2(\gamma k\xi+\phi)]R, \tag{6}$$

with $D=\frac{1}{4}v^2+v\tilde{\alpha}-\tilde{\beta}=-2$. The treatment from Eq. (2) to Eq. (6) is strict without any approximation, since Eq. (3) denotes an exact complete solution of Eq. (2) whose module obeys Eq. (6) strictly. Clearly, Eq. (6) can describe only part properties of the system governed by Eq. (2) and the part properties shared by Eqs. (2) and (6) contain some chaotic features of the system. The uniqueness theorem means that for some definite conditions, the solution of Eqs. (6) and (2) is analytically unique and the same. Under such initial and boundary conditions [e.g., the initial spatial function $\Psi(x,t_0)$ and two boundary time functions $\Psi(\pm x_0,t)$ agree with that of Eq. (3) for the initial time t_0 and boundary coordinate x_0], the numerical computations based on Eq. (2) should also give the same results from Eq. (6). Although it is still hard to find the exact solution of Eq. (6), we can easily obtain its numerical solutions. In fact, the choice $C=0$ leads Eq. (6) to the driven Duffing equation, whose chaotic features have been extensively studied for the single lattice case [23,24]. For our double lattice case, by taking the parameters and initial-boundary conditions $C=0$, $g_1=-0.5$, $D=-2$, $\tilde{V}_1=0.9$, $\tilde{V}_2=0.8$, $\gamma=2$, $\phi=0$, $[R(\xi_0=0),R_\xi(\xi_0=0)]=(-4.01124, -0.626637)$, we plot the Poincaré sections on the equivalent phase space (R,R_ξ) and find the chaotic attractor as in Fig. 1(a). Here, $\xi_0=k_0(x_0+v_Lt_0)$ is the combination of the initial time and boundary coordinate and $\xi_0=0$ means that at a fixed initial time t_0, we take the boundary position $x_0=-v_Lt_0$. When the strength of second lattice is decreased to $\tilde{V}_2=0.2$ and the other parameter values are kept, the Poincaré section becomes regular, as in Fig. 1(b). In both figures, the used driving is strong enough compared to the interaction strength.

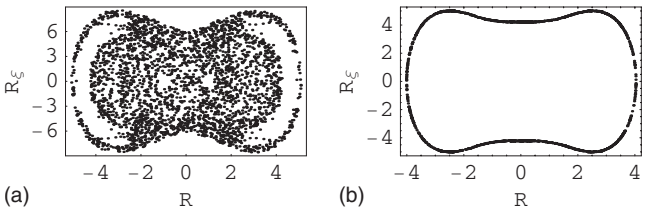

FIG. 1. Plots of the orbits in the equivalent phase space (R,R_ξ) for $C=0$, $g_1=-0.5$, $D=-2$, $\tilde{V}_1=0.9$, $\gamma=2$, $\phi=0$, $[R(\xi_0),R_\xi(\xi_0)]=(-4.011\,24,-0.626\,637)$ and (a) $\tilde{V}_2=0.8$ and (b) $\tilde{V}_2=0.2$. The confuse points in Fig. 1(a) and closed curve in Fig. 1(b) correspond to chaotic and regular orbits, respectively.

We are interested in the weak driving case in which we can find the chaotic properties analytically from Eq. (6) by using the Melnikov-function method [1,30] or/and direct perturbation approach [31]. This weak-field assumption, of course, differs from the tight-binding approximation with strong lattice depths [32]. Regarding the weak V_{op} term as perturbation, the unperturbed part of Eq. (2) is the standard NLSE. Here we consider only the well-known single soliton of the NLSE in the form of Eq. (3) with [33,34] $\theta=-(v/2+\tilde{\alpha})\xi$ due to $C=0$. Comparing to the multisoliton solution, only the single-soliton solution obeys ordinary differential equation (6), so it can be used to fit the Melnikov chaos criterion and to show the transition probability from soliton to chaos analytically. We expand R to the first order,

$$R(\xi) = R_0(\xi) + R_1(\xi), \quad |R_0| \gg |R_1|, \tag{7}$$

and insert it into Eq. (6) with $C=0$, obtaining the zeroth-order and first-order equations

$$\frac{d^2R_0}{d\xi^2} + DR_0 - g_1R_0^3 = 0, \tag{8}$$

$$\frac{d^2R_1}{d\xi^2} + DR_1 - 3g_1R_0^2R_1 = \varepsilon(\xi),$$

$$\varepsilon(\xi) = [\tilde{V}_1 \cos^2(k\xi) + \tilde{V}_2 \cos^2(\gamma k\xi + \phi)]R_0. \quad (9)$$

If the atom-atom interactions are attractive, the system has a negative s-wave scattering length to make $g_1<0$ such that Eq. (8) with a negative D has the well-known homoclinic solution

$$R_0(\xi) = \sqrt{\frac{2D}{g_1}}\,\mathrm{sech}[\sqrt{-D}(\xi + c_0)],$$

$$c_0 = \frac{1}{\sqrt{-D}}\mathrm{arc\ sech}\left[\sqrt{\frac{g_1}{2D}}R_0(\xi_0)\right] - \xi_0. \quad (10)$$

Here, c_0 denotes an integration constant determined by the boundary and initial conditions. Obviously, inserting R_0 of Eq. (10) and $\theta=-(v/2+\tilde{\alpha})\xi$ due to $C=0$ into Eq. (3), we obtain the well-known bright soliton solution [33,34] of the unperturbed NLSE. Applying Eq. (10) to Eq. (9), we construct the general solution of Eq. (9) in the integral form [31]

$$R_1 = h\int_P^\xi f\varepsilon(\xi)d\xi - f\int_Q^\xi h\varepsilon(\xi)d\xi, \quad (11)$$

where P and Q are the integration constants and $f=dR_0/d\xi$ and $h=f\int f^{-2}d\xi$ are two linearly independent solutions of Eq. (9) for $\varepsilon(\xi)=0$,

$$f = \sqrt{\frac{2}{-g_1}}D\,\mathrm{sech}[\sqrt{-D}(\xi + c_0)]\tanh[\sqrt{-D}(\xi + c_0)],$$

$$h = -\frac{\sqrt{-2g_1}}{8(-D)^{3/2}}\mathrm{sech}[\sqrt{-D}(\xi + c_0)]\tanh[\sqrt{-D}(\xi + c_0)]$$
$$\times\{6\sqrt{-D}(\xi + c_0) - 4\coth[\sqrt{-D}(\xi + c_0)]$$
$$+ \sinh[2\sqrt{-D}(\xi + c_0)]\}. \quad (12)$$

Generally, the corrected solution (11) is unbounded because of the unboundedness of h at $\xi=\infty$. However, using the l'Höpital rule, we can easily obtain the sufficient and necessary boundedness condition [31]

$$I_\pm = \lim_{\xi\to\pm\infty}\int_P^\xi f\varepsilon(\xi)d\xi = 0. \quad (13)$$

It is worth noting that the relation between the Melnikov function $M(c_0)$ and Eq. (13) is $M(c_0)=I_+-I_-=\int_{-\infty}^{+\infty}f\varepsilon(\xi)d\xi$. Combining $\varepsilon(\xi)$ in Eq. (9) with R_0 in Eq. (10) and f in Eq. (12) to the integrand, we yield the well-known Melnikov chaos criterion [30]

$$M(c_0) = \frac{2k^2\pi}{g_1}\left[\tilde{V}_1\,\mathrm{csch}\left(\frac{k\pi}{\sqrt{-D}}\right)\sin(2c_0k)\right.$$
$$\left. + \tilde{V}_2\gamma^2\,\mathrm{csch}\left(\frac{\gamma k\pi}{\sqrt{-D}}\right)\sin(2c_0\gamma k - 2\phi)\right] = 0, \quad (14)$$

which indicates the existence of chaos for some c_0 values. Under the conditions of Eqs. (13) and (14), we can call Eq. (11) the "chaotic solution." Thus combining Eqs. (10) and (11) with Eq. (7) produces the chaotic bright soliton solution which is the superposition between the soliton and chaotic states and propagates with the velocity of traveling superlattice.

III. CHAOS PROBABILITIES AND REGIONS

The Melnikov function is a periodic function of c_0 for the fixed parameters and rational number γ, so only the discrete zero points $c_0=c_{0i}$ for $i=1,2,\ldots$ satisfy the chaos criterion $M(c_{0i})=0$. Nevertheless, c_0 is an integration constant depending on the initial and boundary conditions and cannot be accurately set in experiment. When the stochastic initial and boundary conditions are applied to make numerically N' Poincaré sections with N' integer, from Eq. (10), we know that c_0 takes c_{0i} values with only a certain probability, which results in the number n' of chaotic attractors being less than N'. Defining the probability P from soliton to chaos as the ratio n'/N', it is clear that the $P=n'/N'$ value should be related to the number n of c_{0i} in one period of $M(c_0)$ and is always smaller than 1. Taking the chaos probability of single lattice case as the referential one P_0, we have the relation $P=G(n)P_0$ with $G(n)$ being a increasing function of n.

Now let us see how the chaos probability depends on the parameter regions. As a simple example, we first consider the case $\phi=0$ and $\gamma=N\geq 2$ with N integer. We rewrite Eq. (14) in the form

$$M(c_0) = \eta X_1(c_0)X_N(c_0) = 0, \quad (15)$$

where $\eta=2k^2\pi/g_1$, $X_1(c_0)=\sin(2c_0k)$, and $X_N(c_0)=\tilde{V}_1\,\mathrm{csch}(k\pi/\sqrt{-D})+F_N(c_0)$, with $F_N(c_0)=\tilde{V}_2N^2\times\mathrm{csch}(\frac{Nk\pi}{\sqrt{-D}})\frac{\sin(N2c_0k)}{\sin(2c_0k)}$. Clearly, $X_N(c_0)$ is a periodic function of c_0. It has different numbers of zero points in different parameter regions, which can lead to different numbers n of c_{0i} and different chaos probabilities. This can be easily evidenced in the case $N=2$. The superlattice of Eq. (1) with $\gamma=2$ has be widely studied [27]. In such a case, the $X_N(c_0)$ becomes $X_2(c_0)=\tilde{V}_1\,\mathrm{csch}(k\pi/\sqrt{-D})+8\tilde{V}_2\,\mathrm{csch}(2k\pi/\sqrt{-D})\cos(2c_0k)$ and $M(c_0)$ has period π. Obviously, two parameter regions with different zero points of $X_2(c_0)$ exist and the boundary between them is given by

$$\tilde{V}_2 = \tilde{V}_{2b} = \frac{\tilde{V}_1\,\mathrm{csch}(k\pi/\sqrt{-D})}{8\,\mathrm{csch}(2k\pi/\sqrt{-D})} = \frac{\tilde{V}_1}{4}\cosh\frac{k\pi}{\sqrt{-D}}. \quad (16)$$

As an instance from Eq. (16) with $D=-2$, $\tilde{V}_1=0.04$ the boundary curve on the parameter plane $(k,\tilde{V}_2)$ is plotted as in

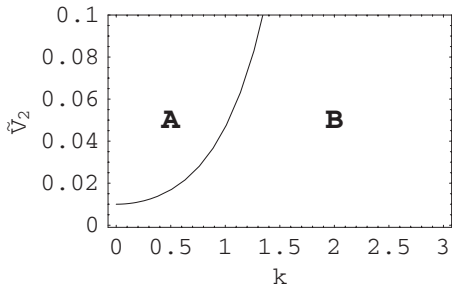

FIG. 2. Plot of the chaotic regions of $\tilde{V}_2$ vs k for the dimensionless parameters $\gamma=2$, $D=-2$, and $\tilde{V}_1=0.04$.

Fig. 2. The region A above the boundary curve is associated with $\tilde{V}_2>\tilde{V}_{2b}$ and the region B below the boundary curve corresponds to $\tilde{V}_2<\tilde{V}_{2b}$.

In order to show the different numbers n of zero point c_{0i} in one period of $M(c_0)$ for the different parameter regions, we make the sketch maps showing the zero points of functions $X_1(c_0)$, $X_2(c_0)$, and $M(c_0)$ as in Fig. 3. For the single lattice case with $\tilde{V}_2=0$ from Fig. 3(a), we see that $X_2(c_0)$ =constant, $M(c_0)$ and $X_1(c_0)$ have the same two $(n=2)$ zero points, indicating the chaos probability $P=G(n)P_0=nP_0/2$ $=P_0$. In Fig. 3(b) with parameters of region A, we exhibit that both $X_1(c_0)$ and $X_2(c_0)$ have two zero points in range $c_0\in[0,\pi)$, respectively, and all the zero points are not coincident. This means that $n=4$ and the chaos probability P $=nP_0/2=2P_0$ in region A. On the boundary between regions A and B, from Fig. 3(c), we can see that two zero points coincide among the three zero points of $X_1(c_0)$ and $X_2(c_0)$ in one period. Therefore, we have $n=2$ and $P=P_0$ on the boundary curve. The same chaos probability appears in region B, which is illustrated by Fig. 3(d), where $X_2(c_0)$ has no zero point and the number $n=2$ of zero points of $M(c_0)$ agrees with that of $X_1(c_0)$.

The above results can be classified as the two cases:

Case 1. In the double chaotic region A with parameters obeying $\tilde{V}_2>\tilde{V}_{2b}$, the chaos probability reads $P=2P_0$;

Case 2. In the chaotic region B and on the boundary curve with parameters obeying $\tilde{V}_2\leq\tilde{V}_{2b}$, the chaos probability equates the referential one, $P=P_0$.

To numerically confirm the analytical results, we use a MATHEMATICA code [35] to make two groups of Poincaré sections on the equivalent phase space (R,R_ξ) for the parameters used in Figs. 3(b) and 3(d) and for the random initial conditions in regions $\{R(\xi_0)\in[-2.1,2.1],R_\xi(\xi_0)$ $\times\in[-2.2,2.2]\}$ associated with a suitable range of c_0. Each of the section groups contains 500 Poincaré sections. For the parameters in region A, 180 chaotic attractors are found and the number of chaotic attractors is 85 for the parameters in region B. The numerical results show that in the chaotic region B, the chaos probability reads $P=P_0=85/500=0.17$ and in the double chaotic region A, the chaos probability becomes $P=180/500=0.36\approx 2P_0$. They well agree with the analytical assertion. The small difference exists between the analytical and numerical results and because of that the strict chaos probability requires more samplings of the Poincaré sections than the used ones.

Then, we take $\phi=0$ and $\gamma=N=3,4,5$ into account and find that for any N, the parameter space can be divided into several parts with different chaos probabilities. Moreover, the number of chaotic regions increases with N and the chaos probability $P=G(n)P_0$ raises as the increase of the zero-point number n. The lowest chaos probability is P_0 and the highest one is associated with the largest zero-point number.

Now we seek the numerical solutions directly from GPE (2). For simplicity and convenience of numerical calculations, we transform Eq. (2) into the equivalent form

$$i\left(\frac{\partial\Psi}{\partial t}+v\frac{\partial\Psi}{\partial\xi}\right)=-\frac{\partial^2\Psi}{\partial\xi^2}+g_1|\Psi|^2\Psi+[\tilde{V}_1\cos^2(k\xi)+\tilde{V}_2\cos^2(\gamma k\xi+\phi)]\Psi, \quad (17)$$

through the variable transformation from (x,t) to (ξ,t). Here time t has been rescaled by unit $\hbar/E_{r0}$ and the dimensionless variables and parameters are the same with Eq. (6). Usually, a numerical solution is associated with a set of fixed initial and boundary conditions. For the definite conditions with the fixed initial solution $\Psi(\xi,t_0)$ and boundary ones $\Psi(\pm\xi_0,t)$, the regular solutions of Eqs. (2), (6), and (17) are analytically the same and unique. However, in chaotic dynamics, it is well known that in the chaotic parameter region the numerical solutions of the same equation can be completely different for two experimentally indistinguishable initial data because of the sensitive dependence of chaos on the initial conditions and computational algorithms [36]. Hence, the numerical results of Eq. (17) can only qualitatively agree with that of Eq. (6), since the chaotic solution of Eq. (6) cannot be determined accurately. If the initial $\Psi(\xi,t_0)$ and boundary $\Psi(\pm\xi_0,t)$ are from the chaotic solutions of Eqs. (6) and (3), the numerical solutions of Eq. (17) are certainly chaotic. Unfortunately, we can obtain the chaotic numerical solutions of Eq. (6) only with a certain probability, which means the existence of the corresponding chaos probability in the numerical simulations of Eq. (17). We apply the semi-

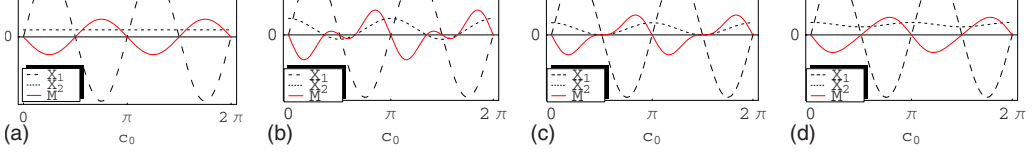

FIG. 3. (Color online) Sketch maps of functions $X_1(c_0)$ (dashed curve), $X_2(c_0)$ (doted curve), and $M(c_0)$ (solid curve) vs c_0 for the parameters $\gamma=2$, $D=-2$, $g_1=-0.5$, $k=1$, and $\tilde{V}_1=0.04$ and (a) $\tilde{V}_2=0$, (b) $\tilde{V}_2=0.08>\tilde{V}_{2b}$, (c) $\tilde{V}_2=0.01\cosh(\pi/\sqrt{2})=0.0466\approx\tilde{V}_{2b}$, and (d) $\tilde{V}_2=0.01<\tilde{V}_{2b}$, where for each different function, the different amplitude scale is adopted for showing the zero points.

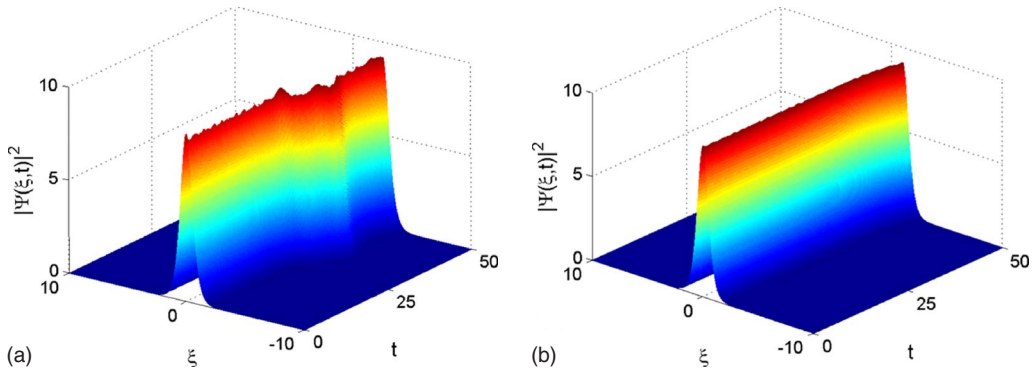

FIG. 4. (Color online) Numerical simulations of Eq. (17) for the spatiotemporal evolutions of the atomic density $|\Psi(\xi,t)|^2$. (a) Chaotic orbit is shown for the parameters of double chaotic region A. (b) Periodic orbit is observed for the parameters of low chaotic region B. In both cases, the initial and boundary conditions are taken as $\Psi(\xi,0)=3\ \mathrm{sech}(1.5\xi)e^{-i0.1\xi}$ and $\Psi(\pm\infty,t)=0$. The space-time coordinate $\xi(x,t)$ is the function with variables x and t being in units of $k_0^{-1}=1/6$ μm and $\hbar/E_{r0}=20$ μs, respectively, and the density is normalized by $100k_0=0.6\ (\mathrm{nm})^{-1}$.

implicit Crank-Nicholson method to perform the numerical simulations directly from Eq. (17). In the case $\gamma=2$, $\phi=0$, by taking the different parameters and the different initial and boundary functions $\Psi(\xi,t_0)=\Psi(\xi,0)$ and $\Psi(\pm\xi_0,t)=\Psi(\pm\infty,t)$, the aperiodic chaotic orbits are found with a certain probability, which are related to the chaos probability based on Eq. (6) qualitatively. The numerical results associated with the definite conditions $\Psi(\xi,0)=3\ \mathrm{sech}(1.5\xi)e^{-i0.1\xi}$ and $\Psi(\pm\infty,t)=0$ and the parameters $g_{1d}=2\hbar\omega_r a_s=-4.34\times10^{-39}$ J m, $V_1=0.04E_{r0}$ are shown in Fig. 4 for (a) $V_2=0.16E_{r0}$ and (b) $V_2=0.01E_{r0}$. Here, we have chosen the initial solution as the zeroth-order approximate soliton of Eq. (2) with $V_{op}=0$, in which $\xi(x,0)$ and Ψ are in units of k_0^{-1} and $100k_0$, respectively. In Fig. 4(a), we observe the aperiodic chaotic density profile for the double chaotic region A of Fig. 2. The regular density profile is exhibited in Fig. 4(b) for the low chaotic region B. The numerical results agree with the above-mentioned analytical ones qualitatively.

IV. CONCLUSIONS

In conclusion, we have investigated a BEC system loaded into a weak moving optical superlattice created by the interference between two lattices with different depths and wave vectors. By applying the Melnikov-function method and the direct perturbation approach, we have demonstrated that the superlattice separates the chaotic region into several parts with different chaos probabilities. The analytical results have been confirmed numerically from the ordinary differential equation (6) and partial differential equation (2), respectively. Moreover, we found that for a fixed first lattice, the modulation of the secondary lattice can transform the chaos probability to zero or a higher one. Controlling the chaos probability to zero is important for the case one requires suppressing chaos. On the other hand, for the secure chaos-based cryptosystems, one calls for higher chaotic probability. Given the above-mentioned results, we can weaken or strengthen chaos by adjusting the parameters into different chaotic regions.

When the zero traveling velocity $v_L=0$ is set, the results directly fit the corresponding static BEC system. The used method could also be easily extended to the investigation of temporal chaotic systems with double-frequency driving.

ACKNOWLEDGMENTS

The authors thank Dr. X. Luo for the help in numerical simulation. This work was supported by the National Natural Science Foundation of China under Grants No. 10575034 and No. 10875039.

[1] F. Kh. Abdullaev and R. A. Kraenkel, Phys. Rev. A **62**, 023613 (2000).
[2] P. Coullet and N. Vandenberghe, Phys. Rev. E **64**, 025202(R) (2001).
[3] C. Zhang, J. Liu, M. G. Raizen, and Q. Niu, Phys. Rev. Lett. **93**, 074101 (2004).
[4] J. Denschlag, J. E. Simsarian, D. L. Feder, Charles W. Clark, L. A. Collins, J. Cubizolles, L. Deng, E. W. Hagley, K. Helmerson, W. P. Reinhardt, S. L. Rolston, B. I. Schneider, and W. D. Phillips, Science **287**, 97 (2000).
[5] K. E. Strecker, G. B. Partridge, A. G. Truscott, and R. G. Hulet, Nature (London) **417**, 150 (2002).
[6] F. Kh. Abdullaev and R. Galimzyanov, J. Phys. B **36**, 1099 (2003).
[7] T. Mayteevarunyoo, B. A. Malomed, and M. Krairiksh, Phys. Rev. A **76**, 053612 (2007).
[8] K. Nozaki and N. Bekki, Phys. Rev. Lett. **50**, 1226 (1983).
[9] H. T. Moon and M. V. Goldman, Phys. Rev. Lett. **53**, 1821 (1984).
[10] R. Scharf and A. R. Bishop, Phys. Rev. A **46**, R2973 (1992).
[11] P. V. Elyutin, A. V. Buryak, V. V. Gubernov, R. A. Sammut, and I. N. Towers, Phys. Rev. E **64**, 016607 (2001).

[12] F. Kh. Abdullaev, E. N. Tsoy, B. A. Malomed, and R. A. Kraenkel, Phys. Rev. A **68**, 053606 (2003).
[13] A. D. Martin, C. S. Adams, and S. A. Gardiner, Phys. Rev. Lett. **98**, 020402 (2007).
[14] R. Roth and K. Burnett, J. Opt. B 5, S50 (2003).
[15] C. C. Huang and W. C. Wu, Phys. Rev. A **72**, 065601 (2005).
[16] L. Sanchez-Palencia and L. Santos, Phys. Rev. A **72**, 053607 (2005).
[17] A. A. Sukhorukov, Phys. Rev. Lett. **96**, 113902 (2006).
[18] J. E. Lye, L. Fallani, C. Fort, V. Guarrera, M. Modugno, D. S. Wiersma, and M. Inguscio, Phys. Rev. A **75**, 061603(R) (2007).
[19] D. Shechtman, I. Blech, D. Gratias, and J. W. Cahn, Phys. Rev. Lett. **53**, 1951 (1984).
[20] J. Denschlag, J. E. Simsarian, H. Häfner, C. McKenzie, A. Browaeys, D. Cho, K. Helmerson, S. L. Rolston, and W. D. Phillips, J. Phys. B **35**, 3095 (2002).
[21] L. Fallani, F. S. Cataliotti, J. Catani, C. Fort, M. Modugno, M. Zawada, and M. Inguscio, Phys. Rev. Lett. **91**, 240405 (2003).
[22] B. Eiermann, Th. Anker, M. Albiez, M. Taglieber, P. Treutlein, K. P. Marzlin, and M. K. Oberthaler, Phys. Rev. Lett. **92**, 230401 (2004).
[23] G. Chong, W. Hai, and Q. Xie, Phys. Rev. E **70**, 036213 (2004).
[24] F. Li, W. Shu, J. Jiang, H. Luo, and Z. Ren, Eur. Phys. J. D **41**, 355 (2007).
[25] K. M. Cuomo and A. V. Oppenheim, Phys. Rev. Lett. **71**, 65 (1993).
[26] Xiaowen Li, Heqiao Zhang, Yu Xue, and Gang Hu, Phys. Rev. E **71**, 016216 (2005).
[27] P. J. Y. Louis, E. A. Ostrovskaya, and Y. S. Kivshar, Phys. Rev. A **71**, 023612 (2005).
[28] S. A. Gardiner, D. Jaksch, R. Dum, J. I. Cirac, and P. Zoller, Phys. Rev. A **62**, 023612 (2000).
[29] W. Miller, *Symmetry and Separation of Variables* (Addison-Wesley, London, 1977).
[30] V. K. Melnikov, Trans. Mosc. Math. Soc. **12**, 1 (1963).
[31] W. Hai, C. Lee, G. Chong, and L. Shi, Phys. Rev. E **66**, 026202 (2002); C. Lee, W. Hai, L. Shi, X. Zhu, and K. Gao, Phys. Rev. A **64**, 053604 (2001); W. Hai, X. Liu, J. Fang, X. Zhang, W. Huang, and G. Chong, Phys. Lett. A **275**, 54 (2000).
[32] V. Ahufinger, A. Sanpera, P. Pedri, L. Santos, and M. Lewenstein, Phys. Rev. A **69**, 053604 (2004).
[33] A. Hasegawa and Y. Kodama, *Soliton in Optical Communications* (Clarendon Press, Oxford, 1995).
[34] B. Guo and X. Pang, *Solitons* (Science Press, Beijing, 1987), p. 8 (in Chinese).
[35] Q. Zhu, W. Hai, and S. Rong, e-print arXiv:0804.0906.
[36] J. Ford, in *The New Physics*, edited by P. Davies (Cambridge University Press, Cambridge, England, 1989).